NORDA Technical Note 179

Naval Ocean Research and
Development Activity,
NSTL Station, Mississippi 39529

K-Band Radiometric Mapping of Sea Ice

R. D. Ketchum, Jr.
L. D. Farmer
J. P. Welsh, Jr.

Oceanography Division
Ocean Science and Technology Laboratory

January 1983

ABSTRACT

The Ka-band radiometric mapping system (KRMS), an airborne 33.6 GHz passive microwave imager, was flown over sea ice in the Bering, Chukchi and Beaufort Seas and in the Canadian Archipelago. The data discussed was obtained on 14 and 16 May 1982. The system, as flown, measures the relative brightness temperature (T_B) of the objects radiating toward the rotating antennae. Differences in T_B appear to be related to variation in ice thickness, surface moisture, deformation processes and melting and refreezing processes. A snow/ice interface development is hypothesized to relate to decreasing T_B as ice increases in age.

The T_B of undisturbed new ice is warmer than open water. The T_B of first-year ice appears to decrease with increasing age and seems to be less variable than the thinner ice types.

Multi-year ice appears colder than first-year ice but warmer than open water. Two different categories of multi-year ice floes were observed. Arctic basin multi-year floes were distinguished by the rounded shapes, colder T_B and irregular distribution of frozen melt ponds (warmer T_B). Archipelago multi-year floes were less rounded, had warmer T_B and displayed a more regular (homogeneous) distribution of frozen melt ponds. Both categories of multi-year floes were radiometrically colder than the warmer (higher T_B) first-year ice types surrounding them and thus were readily identified.

New ice ridges were not unambiguously identified on the imagery. Ice ridges were inferred because of the observed association with warm lineations on the KRMS imagery when the ridge feature was clearly distinguished on the simultaneously obtained aerial photograph.

The imagery (hard copy) was produced in near real time, with 16 gray levels, onboard the aircraft in flight. Future processing will be digital with 256 gray levels and performed on an interactive digital image processing system.

ACKNOWLEDGMENTS

This project was funded by ONR Code 420, Charles Luther, manager, under Program Element 61153N.

K-BAND RADIOMETRIC MAPPING OF SEA ICE

Introduction

In April 1976, the prototype Ka-band (33 GHz) radiometric mapping system (designated as MICRAD for microwave imaging radiometer in 1976) was flown over sea ice in the Chukchi and Beaufort Seas. The results of the mission (Ketchum and Lohanick, 1980) were very encouraging to sea ice investigators who saw the potential of this or similar all-weather microwave systems in future sea ice research and operational programs.

Basically, this system provided high resolution image maps of the distribution of relative brightness temperatures (T_B) which could be used to classify ice into various types and open water. Areas of open water, first season ice, and old ice were easily discriminated. The first season ice could be further discriminated or divided into categories. The data suggested that the ice became radiometrically colder with increasing age. New ice ridges could not be detected in a field of first-year ice, but could be inferred in older (multi-year) ice from their association with radiometrically warm lineations. However, the lineations were often observed to represent narrow frozen fractures as well as new ridges.

The new Ka-band (33 GHz) radiometric mapping system (KRMS) is an improved version of the prototype unit flown in 1976. Improvements to the system's electronics have been made and the system has been pod mounted for installation on different aircraft. The pod mounted assembly was originally designed for wing installation on fleet P-3C aircraft. To evaluate and develop the imagery interpretation capability, RP-3A aircraft (Oceanographic Development Squadron Eight, VXN-8) have been modified to carry the pod suspended beneath the bomb bay area (Fig. 1). Wing installation on the RP-3A was not possible because the wings were not stressed for the load and adequate hard points were not available for wing stores. The VXN-8 RP-3As can be equipped with a cartographic camera, infrared line scanner, laser surface profiler, precision radiation thermometers and various meteorological sensors which are complementary to the KRMS.

The KRMS imagery processing equipment can be used onboard the aircraft, in flight, so that near real-time hard copy imagery can be produced. The production of near real-time KRMS imagery permits airdrops to ice properties measurement teams on the surface so that image features can be directly related to the corresponding sea ice features. This near real time observation/measurement procedure will increase understanding of the effect of snow and ice properties on microwave radiation.

The KRMS System

The KRMS, developed by the Naval Weapons Center, China Lake, Calif., operates at a center frequency of 33.6 GHz. Three parabolic vertically polarized antennae with beamwidth of 1.1 degrees rotate about a horizontal axis at speeds of 7-25 scans/second. Each antenna scans 60 degrees either side of nadir. However, only 100 degrees of the available 120 degrees cross track scan is used because of the extreme signal fall-off at the scan extremes. Cross track coverage is equal to 2.38 times the flight altitude. The image is formed by scanning the antenna, and the forward motion of the aircraft. The power supply, antennae, and support electronics are housed in the protective pod. Signal processing and recording components are mounted within the aircraft cabin.

The RF amplifier output is recorded, along with all sensor and flight parameters, on analog tape. The in-flight imaging system consists of an analog-digital display/recording unit. The system processes the analog signal into digital format with storage in a data memory/processing unit. The imaging system output is in a composite video format. The radiometer signals are sampled (nonlinear) and processed to correct geometric distortions, digitized, and read into a microprocessor. The illusion of a moving scene is accomplished by "scrolling" the video output as new data is written into the matrix over the oldest data. The output is produced with 16 gray levels. The system can be expanded to output 256 gray levels to improve image contrast.

The Field Experiment

Data collection flights were made from Elmendorf AFB, Alaska, on 14 and 16 May 1982. Figure 2 shows the general flight tracks used for this study. The 14 May flight crossed over the Beaufort Sea into McClure Strait and Crozier Channel. Flight lines in the vicinity of Mould Bay, Prince Patrick Island, Canada, were flown at 900 m and duplicated lines flown by U. S. and Canadian experimenters during October 1981. KRMS imagery taken over two of these lines has been correlated with Canadian side-looking airborne radar data taken in October 1981. Flight altitudes of 300 m were maintained throughout most of the flight to obtain high resolution photography for correlation with the KRMS imagery. Light snowfall was observed over the Beaufort Sea during the 14 May flight.

Data collection on the 16 May flight was conducted over the Bering Sea from St. Lawrence Island northward through the Bering Strait and continued over the Chukchi Sea. Weather conditions were much the same as on the 14 May flight and altitudes of 300 m were maintained throughout most of the flight. Landfall was made at Pt. Barrow, Alaska, and KRMS data collection was continued over the North Slope to the Brooks Range.

The VXN-8 SEASCAN RP-3A aircraft was the sensor platform used during this mission. In addition to the KRMS, an RC-10 aerial camera, PRT-5 infrared radiometer, low-light level television and laser surface profiling system were operated.

The KRMS was not calibrated during this mission so absolute values of T_B cannot be determined. The images portray the distribution of relative T_B. Colder T_B is represented by the lighter gray tones on the image. The KRMS was modified during August 1982 and is now a calibrated system.

The data used for this preliminary analysis were quick-look hard copy prints produced on the aircraft, in flight, in near real-time during the mission and do not represent the optimum results obtainable. When funds become available, software will be developed to expand and evaluate the full range of analog and digital data. Digital data will be formatted for analysis using NORDA's Interactive Digital Image Processing System.

Results

The KRMS 33 GHz imagery has shown relative brightness temperature distribution as anticipated based on results of the prototype 33 GHz system flown over sea ice in April 1976. However, the new system provides significant improvement in the ability to discriminate first-year ice thicknesses. This improvement can be attributed to greater system sensitivity and increased dynamic range.

Areas of open water display the lowest (coldest) T_B in the Arctic environment. Airborne field measurements have shown open water in the Arctic to be near 140°K at vertical incidence when using a 33 GHz radiometer (Tooma, et al., 1975). Surface measurements using a 33 GHz radiometer (Lohanick, 1982) have indicated a T_B of 150°K at 40° incidence angle. Imaged open water areas are easily identified because they are sharply contrasted against the background ice, which has a much higher (warmer) T_B. New ice types exhibit both high and low T_B. The lower T_B is believed to reflect free water (liquid phase) at the surface. Field measurements (on the ice) using the NORDA 33 GHz radiometer have shown that for initial ice growth up to 2 mm thickness, the T_B increased rapidly (steep slope) to about 200°K. For continued growth (greater than 2 mm thick) the increase slowed (less steep slope) as it approached ambient air temperatures (260K) when the ice was about 13 mm thick (Lohanick, 1981). This latter reading probably approaches a maximum T_B for sea ice at this frequency (33.6 GHz). However, it is reasonable to expect wide and rapid fluctuations of T_B at 33 GHz in very thin ice types because surface conditions, particularly moisture (liquid phase) can be changed abruptly by local atmospheric conditions. Increasing surface moisture will decrease the T_B. Hawkins et al. (1981), using measurements from an airborne 19.4 GHz radiometer, have shown the dependence of T_B on the presence of surface water/moisture.

Figure 3 shows an area of relatively undisturbed new ice just beginning to form on an open fracture. The corner ticks on the KRMS image show the approximate locations of the corners of the coincident photography. The darker tone or warmer T_B of the new ice is clearly evident on the KRMS image. The cooler T_B within the fracture area is believed to be caused by surface moisture in these areas, possibly caused by surface flooding. Figure 4 shows an area of rafted young ice with scattered areas of open water. The open water areas are the radiometrically coldest features. The dark bands in the KRMS image represent the most actively rafted areas, probably more than two layers of rafted ice. Undeformed areas and less actively rafted areas display a cooler (lighter gray tone) radiometric temperature than the most actively rafted ice. Physical temperatures of the surface areas of the thicker rafted ice should be cooler than the thinner, undeformed and less actively rafted areas. It is believed that the T_B differences are influenced by the greater amount of surface moisture in the thinner ice areas. The decrease in emissivity caused by the increased surface moisture more than offsets the effects of the colder surface physical temperatures of the thicker rafted areas. A further indication of the presence of surface moisture is the apparent increase in T_B with incidence angle. Note that the edges of the microwave image (right and left), corresponding to larger incidence angles (at vertical polarization) are darker, indicating higher T_B. This behavior is characteristic of moist surfaces (Grenfell and Lohanick, 1982) and is not noticeable in all the images shown in this study.

The actively rafted area of thin ice in Figure 5 is snow covered. Snow was observed falling when the imagery was taken. Melting of the snow is evident in many places on the photography, particularly near the open water areas. Ice this thin will not maintain a snow cover for long when air temperatures are around -10°C as they were during the flight. Again we see the thicker rafted areas as being radiometrically warm, presumably because snow melt is not as rapid in these areas as it is in the thinner ice areas. The cold brightness temperatures of the thinner unrafted ice are attributed to a wet snow cover.

The preceding discussion, with illustrations, has given some indication of T_B variations which can occur in the very early stages of ice development. Although

speculative, it appears that variations in surface moisture (liquid phase) on thin ice influence the variation in T_B.

Discrimination of variation in thicknesses of first-year ice is possible on the KRMS imagery. Sea ice becomes radiometrically cooler with age and the T_B appears to be more consistent and stable for first-year ice than for the thinner (younger) ice types. The surface physical temperatures are expected to approach the colder ambient air temperatures as the ice grows thicker, since surface temperatures of thicker ice are less affected by conduction from the warmer underlying water. This would suggest a trend of decreasing T_B with increasing ice age. However, it is hypothesized that a snow/ice interface layer is the primary feature controlling the T_B of first-year ice and older sea ice types. The highly porous snow/ice layer acts as a scattering medium which reduces the radiation from the underlying ice. As this snow/ice interface develops with increasing age, there is an apparent corresponding decrease in emissivity. It is postulated that the growth and development of a snow/ice interface layer results in a decrease in the radiometric temperature of sea ice with increasing age, especially for the higher microwave frequencies. Ketchum (1981) has hypothesized that radar systems (X-band) show increasing backscatter when the snow/ice interface layer is sufficiently developed.

The 16 May 1982 Chukchi Sea scene shown in Figure 6 displays variations in first-year ice thickness which are apparent on both the KRMS image and the coincident photography. The thinner first-year ice (A) is depicted as a somewhat homogeneous, relatively high (warm) T_B feature. The flooded area (indicated by arrow) appears radiometrically cool. The thicker first-year ice (B) displays a relatively low T_B and seems to have more variation in T_B than the thinner first-year ice (A). These variations in T_B could be variations of ice thickness which cannot be determined on the photography. Ridges cannot be unambiguously identified in Figure 6.

The scene in Figure 7, taken from 16 May 1982 data in the Chukchi Sea, shows a complex mixture of first-year ice thicknesses with ridging and rubble. Correlating features between the KRMS image and photograph is difficult. Variation in ice thickness, in different areas, is difficult or impossible to interpret from the photograph because of the drifted snow around the ridges and in the rubble. However, on the KRMS image, the distribution of the thinner ice areas (A) is shown by the higher (warmer) T_B.

Signal loss from the ice caused by the snow cover may be anticipated; however, the loss does not appear to be significant. The fragmented nature of the ice in this area (Fig. 7) would suggest intensive ridging and rubble formation. The deformational features cannot be clearly identified on the microwave image, but can be inferred because of the fragmented character of the ice displayed in the image.

Variations in first-year ice thickness shown in Figure 8 are not as evident on the photography as some of those shown in Figures 6 and 7. The long, narrow, snow-covered frozen fracture (arrows pointing to it) is clearly evident on both the KRMS image and the photography. The other thinner ice areas (A) and (A_1) are not readily identified on the photograph without correlation with the KRMS image. This is particularly true of the thinner area at (A_1) because a visible boundary between (A_1) and the adjacent thicker ice (B) is not apparent. Ridges are not directly indicated on the KRMS but can be inferred based on complexity of the ice thickness distribution in the image. Ridges commonly occur at boundaries between areas of different ice thickness.

KRMS imagery in general, does not permit ice ridges and hummocked areas to be directly detected. Signatures associated with ridges are extremely variable. Often ridged areas contrasted (different T_B) against the surrounding ice, and apparently just as often the ridged areas can have the same brightness temperature as the surrounding ice. It is not clear at this stage in the investigation what these signatures represent when a ridge is imaged. Intuitively, it appears that first-year ridges should have a lower T_B than the adjacent undeformed ice from which the ridge was formed. The ice blocks in a ridge which have been raised above the water should be physically colder than (greater surface exposure to colder ambient air temperature) the undeformed floating ice. Brine drainage from the ice blocks in a ridge should produce a more porous medium, thus increased scattering for the 33 GHz frequency. Both these phenomena should result in a lower T_B. It follows then, that the relatively high (warm) T_B observed in the ridge zones do not represent the ridge, but some phenomenon associated with the ridge or the ridging process. The KRMS ridge signature has been observed to be much wider than the ridge as seen on the coincident photography. In some cases, this could be caused by warmer radiation from the adjacent undeformed portions of the ice covered fracture from which the ridge was formed. Often this undeformed area cannot be seen on the photography because of deep snow drifts along the ridge. Other factors which must be considered to explain the ridge signature are the apparent radiation reducing effects of ice surface flooding (surface moisture) and deep drifted snow associated with ridges.

The network of ridges seen in Figure 9 lie in an area of relatively homogeneous thick first-year ice. When comparing the KRMS image and the photograph of these ridges, it becomes clear that factors other than ridge size and age affect the microwave signature. The large sinuous ridge, (A), produces a broad, dark-toned (warm) microwave signature which is three to four times the measured width of this feature on the photograph. Ridge (B), older and smaller than ridge (A), is not continuously observable on the KRMS image. A remnant of the thinner ice-covered fracture from which this ridge was formed is seen as a dark-toned (warm) feature (C) on the KRMS image. Ridge (D), also smaller and older than ridge (A), produces very little contrast in T_B. However, ridge (E), which is smaller than ridges (B) and (D), produces a KRMS signature equivalent to that produced by the much larger ridge (A). Furthermore, the microwave image shows ridge (E) extending into ridge (A). This extension does not show on the photograph. Possibly a snow-covered remnant of the original ice covered fracture from which the ridge was formed lies in this zone.

Figure 10 also shows an area of apparently homogeneous ice thickness with the exception of the more recent ice covered fracture in the upper left corner of the photographed area. The ridges appear much wider on the KRMS image than on the photograph. The ridges appear relatively uniform in width on the photograph, but along with the evidence shown in Figure 9, suggests that the warmer radiation is from a source other than or in addition to the ridges. The source for ridges indicated by (A) in Figure 10, is probably thinner ice adjacent to the ridge which cannot be identified on the photography. Ridge (B) is barely observable suggesting the absence of thinner ice adjacent to this ridge. The ridge at (C) is recent, as indicated by flooding and the absence of drifted snow. The adjacent ice appears to be the older thicker first-year ice which dominates this scene. Much of this ice has been fractured and pushed downward by the weight of the ridge, and subsequently flooded. It is speculated that new ice forming on the flooded area may be responsible for some of the higher (warmer) radiation seen in association with ridge (C). It is clear from the evidence shown in Figures 9 and 10 that radiation from new ice ridges and associated features is very complex, thus requiring additional, more detailed field work.

Figure 11 shows KRMS imagery and coincident photography taken in Crozier Channel on 14 May 1982. Multi-year ice floes are seen frozen in a matrix of first-year ice which in some areas is smooth and in other areas contains rubble. The difference in T_B displayed by the multi-year floes is attributed to the distribution of frozen melt water which has a relatively high (warm) T_B. The light tone floes (A) (colder) with hummocking and ridging are believed to have originated in the Arctic Basin where they experienced intense deformation before entering the archipelago. The ridges and hummocks have restricted the horizontal distribution of the melt water leaving an irregular pattern of dark spots (melt pools) against a bright background. The multi-year ice floes (B) which display a higher (warmer), more homogeneous T_B are believed to have formed within the archipelago. Surface relief on these floes, which is relatively low, is attributed primarily to summer melt and erosional processes. On the photograph, the relief on (B_2) is greater and more irregular than on (B_1). (B_1) shows a higher (warmer) T_B on the KRMS image than (B_2). The lower relief permits a more widespread horizontal distribution of melt water and subsequently, a fresh water ice layer on the surface. The areas, shown as (C), of smooth first-year ice display the highest (warmest) T_B. The rubble in other areas (D) of first-year ice reduces the average T_B suggesting that the rubble is comprised of multi-year ice. These areas often have a homogeneous gray tone similar to the archipelago multi-year ice floes, but can usually be differentiated because of shape differences and well defined edges of the individual floes.

Concluding Remarks

This preliminary analysis of KRMS imagery has shown that there is a rapid increase in T_B as ice begins to grow undisturbed in open water. However, the data suggests that factors such as snow cover and flooding can produce sufficient surface moisture (liquid phase) on thin ice types to effectively reduce the T_B, thus a wide range in T_B should be anticipated with ice types less than 30 cm thick (nilas and young ice). T_B appears to be more consistent for first-year ice than with the thinner ice types. The surface conditions of first-year ice, particularly the thicker stages of development, are not influenced as easily or as rapidly by local weather conditions or deformational activity. First-year ice becomes radiometrically cooler as it gets older. The cooling trend is attributed to a decreasing emissivity which is related to the development of an increasing porosity at the snow/ice interface layer. The snow/ice layer is a scattering medium to high microwave frequencies. The age increasing/radiometrically cooling trend provides for discrimination of relative ice thicknesses in first-year ice types. Surface observations will be necessary to determine if small ranges of first-year ice thickness can be discriminated by differences in T_B. This analysis has indicated that small thickness differences are being sensed, but this judgment is based only on correlative photography, not in situ field measurement of ice thickness.

New ice ridges cannot be routinely identified on the KRMS imagery, but their presence can be inferred at boundaries between areas of different ice thickness. Further analysis of this data using the 256 gray level digital tape generated imagery with computer enhancement techniques may make the ridges more distinct.

Multi-year ice floes are easily identified because of their shapes (rounded) and a relatively cool T_B with irregular patterns of radiometrically warm frozen melt pools. Multi-year ice formed in the Canadian Archipelago can be distinguished from multi-year ice formed in the Arctic Basin because of the more homogeneous distribution of melt water over the surface of the lower relief archipelago ice which increases the overall T_B.

Future work using a calibrated system with coincident surface truth (in situ) measurements including a 33 GHz portable radiometer along with other ice property measurements will result in the necessary correlative data to relate T_B with ice thickness and other ice characteristics.

REFERENCES

Grenfell, A. and A. Lohanick (1982). 1982 Summarized Study Data Report: RADARSAT, Mould Bay, Prince Patrick, NWT Canada. RADARSAT Project Office, Canadian Dept. of Energy, Mines and Rsources.

Hawkins, R. K., A. L. Gray, and C. E. Livingstone (1981). Seasonal Effects on the Microwave Signatures of Beaufort Sea Ice. Proceedings of the Fifteenth International Symposium on Remote Sensing of Environment, Ann Arbor, Mich., v. I, p. 239-257.

Ketchum, R. D., Jr. and A. W. Lohanick (1980). Passive Microwave Imagery of Sea Ice at 33 GHz. Remote Sensing of Environment, v. 9, n. 3, p. 211-223.

Ketchum, R. D. Jr. (1981). Dual Frequency Radar Ice and Snow Signatures. NORDA Technical Note 135.

Lohanick, A. W. (1981). Brightness Temperature of a Freezing Lead at 33 GHz. Proceedings of the Second Workshop on the Microwave Remote Sensing of Sea Ice and Icebergs. Langley Research Center, Hampton, Va.

Lohanick, A. W. (1982). Personal communication.

Tooma, S. G., R. A. Mennella, J. P. Hollinger, and R. D. Ketchum, Jr. (1975). Comparison of Sea-Ice Type Identification Between Airborne Dual-Frequency Passive Microwave Radiometry and Standard Laser/Infrared Techniques. Journal of Glaciology, v., 15, n. 73, p. 225-239.

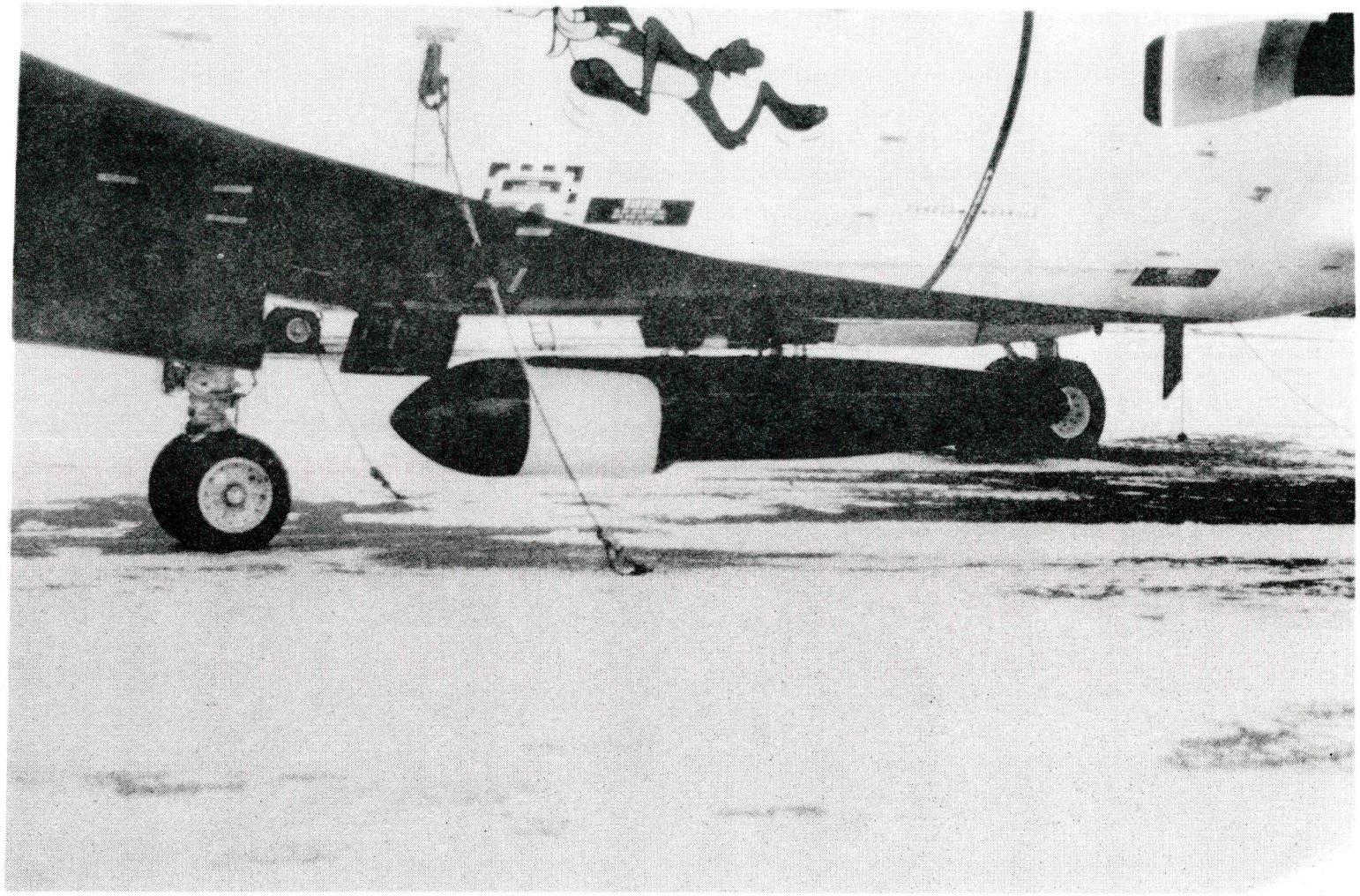

Figure 1. The 4.9 meter long KRMS pod is shown suspended beneath the bomb bay area of the Project SEASCAN RP-3A.

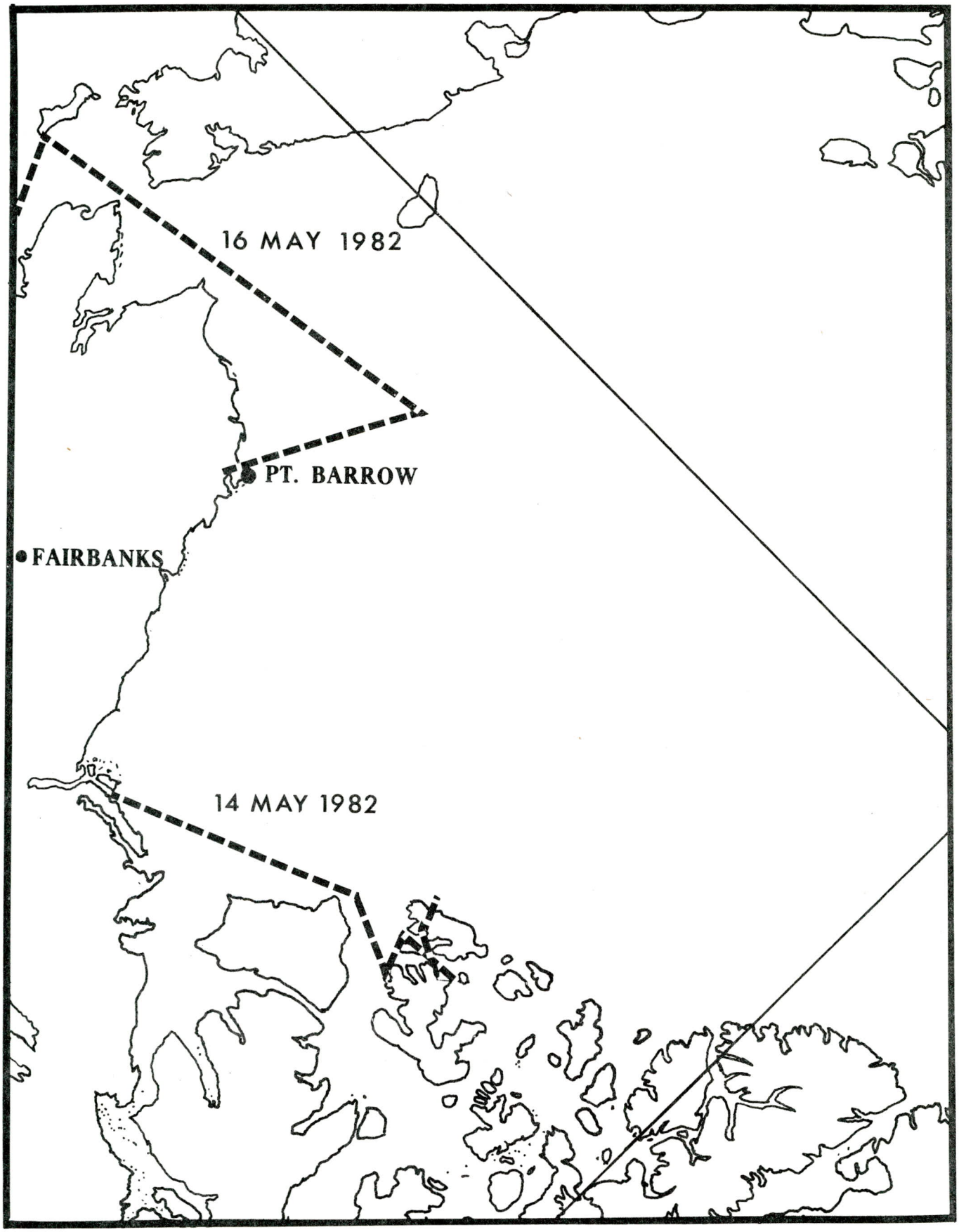

Figure 2. General flight tracks for this study.

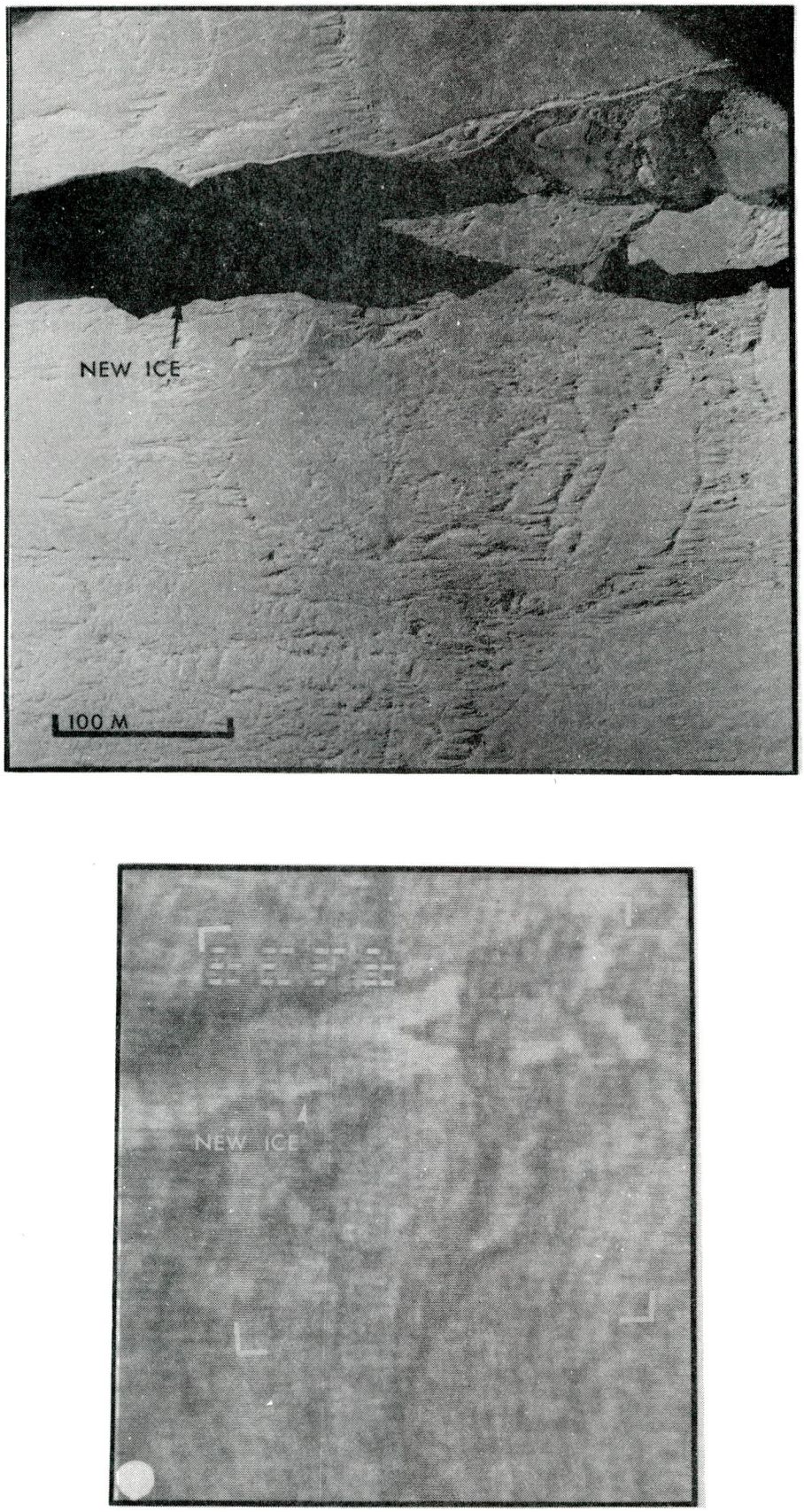

Figure 3. New ice just beginning to form in an open fracture raised the T_B.

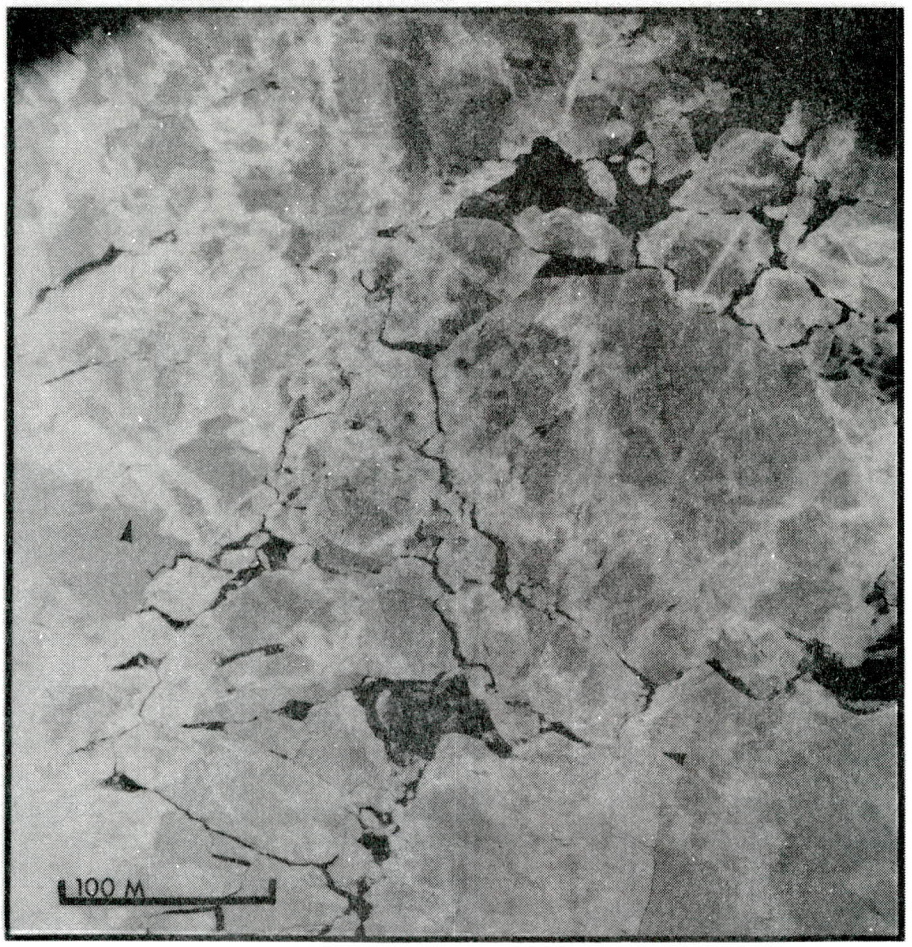

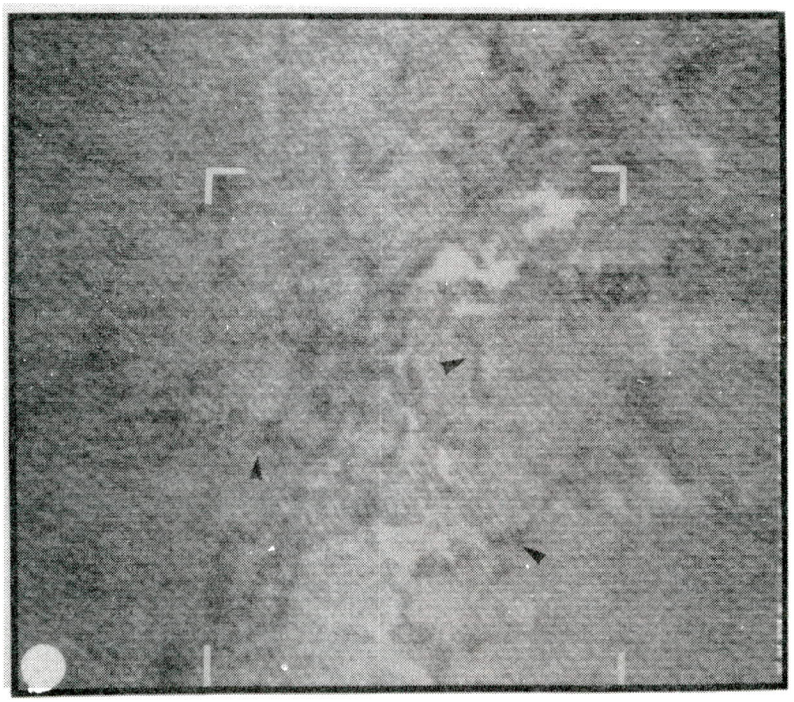

Figure 4. Areas of rafted thin ice show higher T_B than unrafted areas.

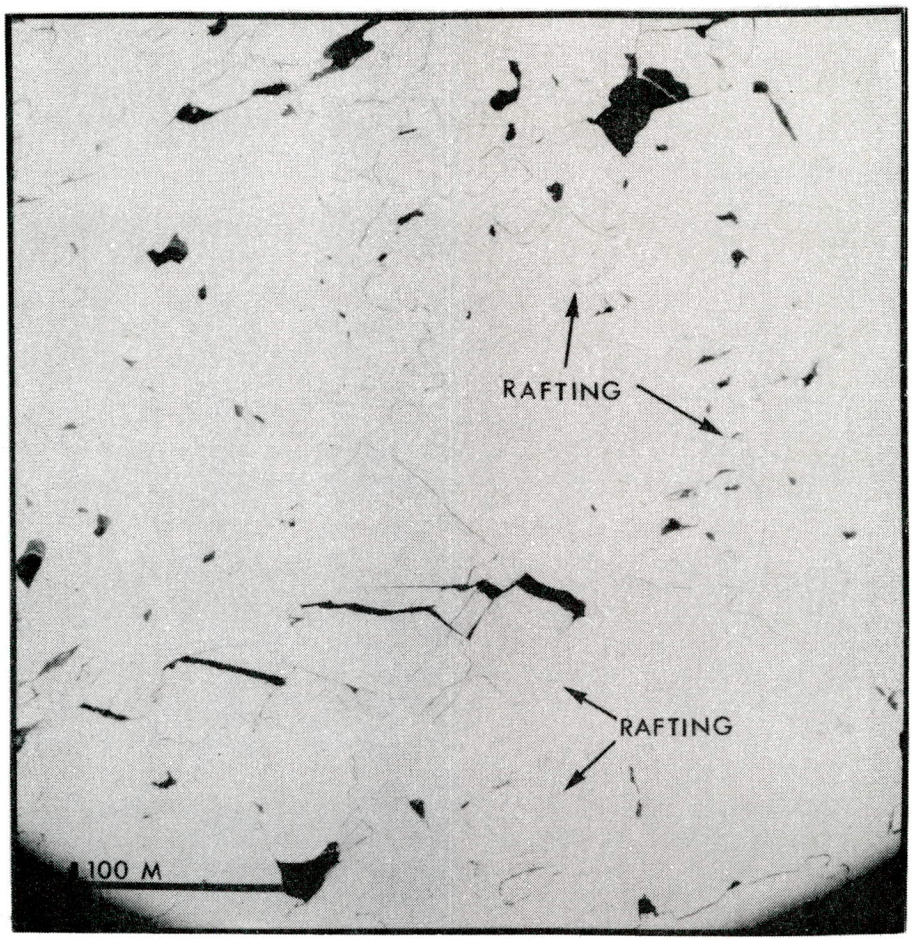

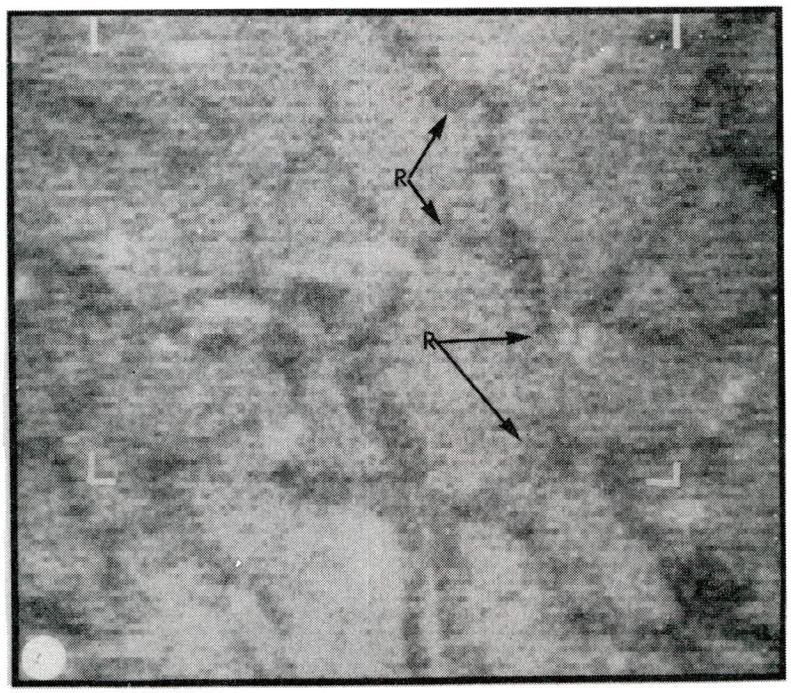

Figure 5. Reduced T_B of thin ice is attributed to wet snow. Thicker rafted areas of ice appear radiometrically warmer.

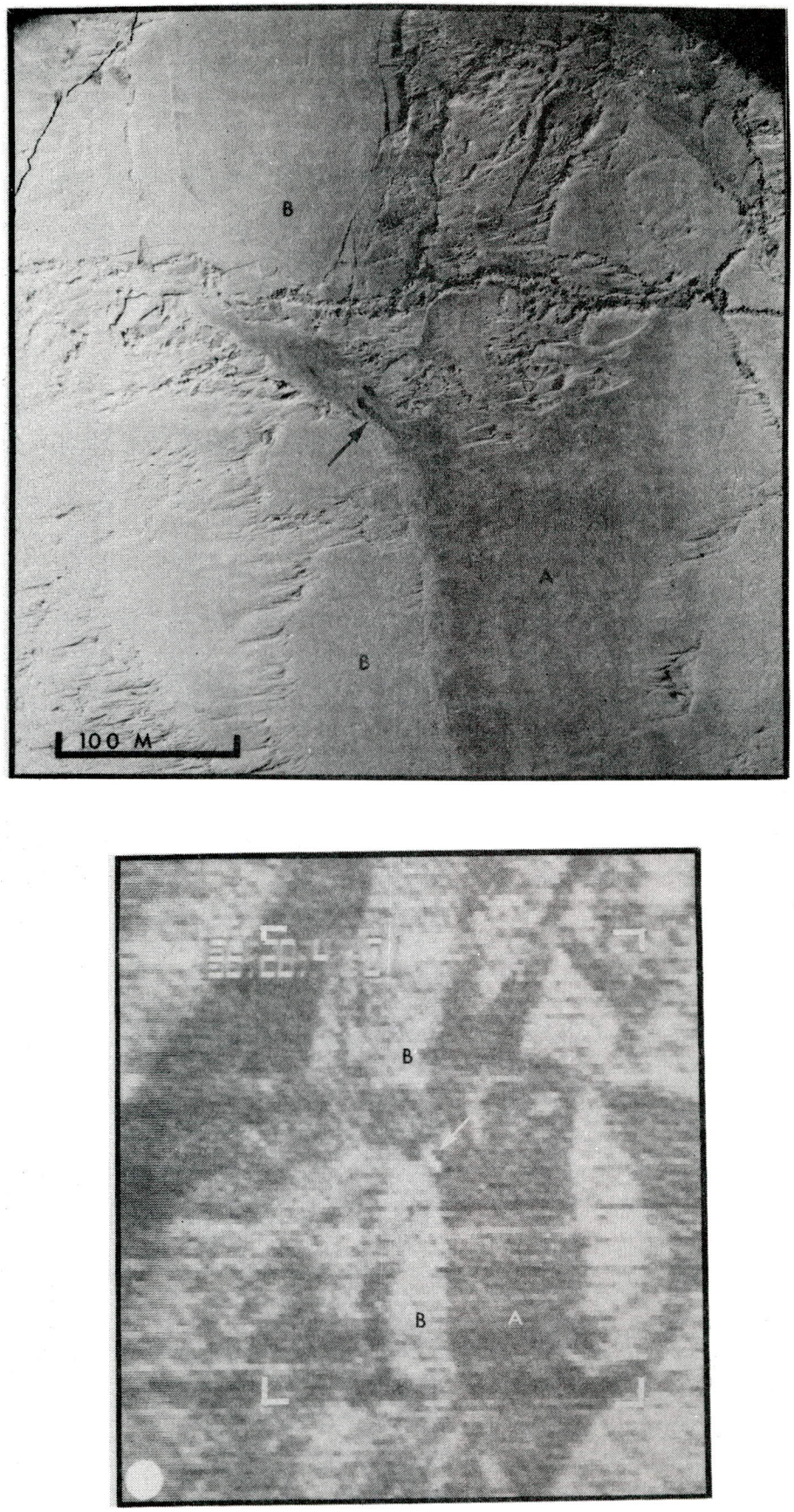

Figure 6. First-year (FY) ice thicknesses are discriminated by T_B. The dark-toned thinner areas, like (A), are radiometrically warmer.

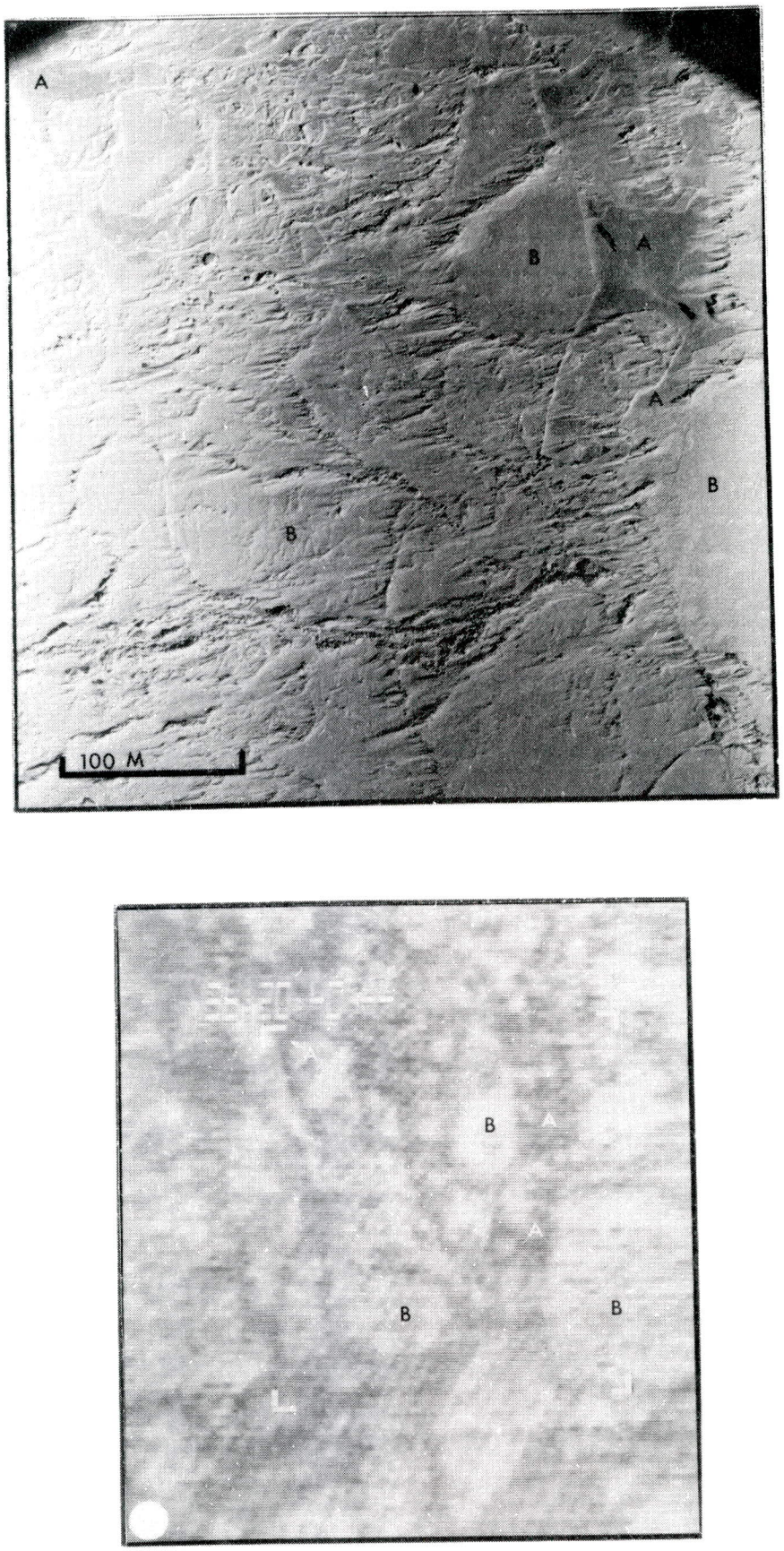

Figure 7. The tonal variations on the KRMS image allow discrimination of the radiometrically warmer thinner ice areas in this complex scene. Heavy snow cover prevents much of this discimination on the photography.

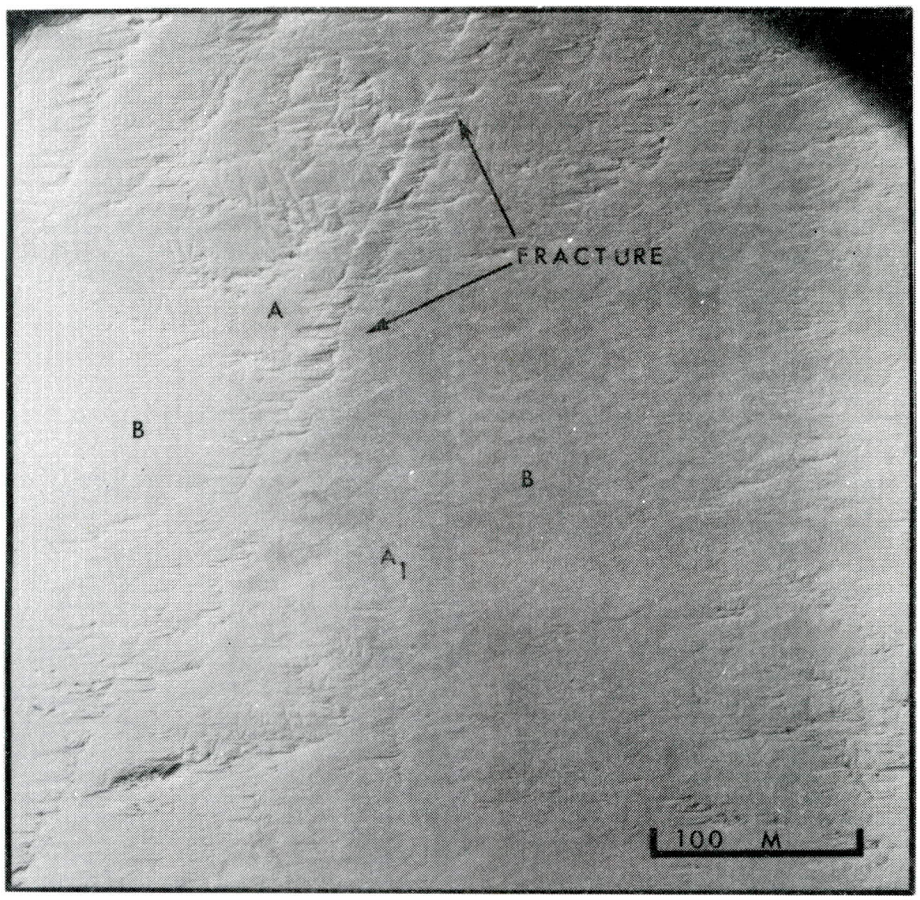

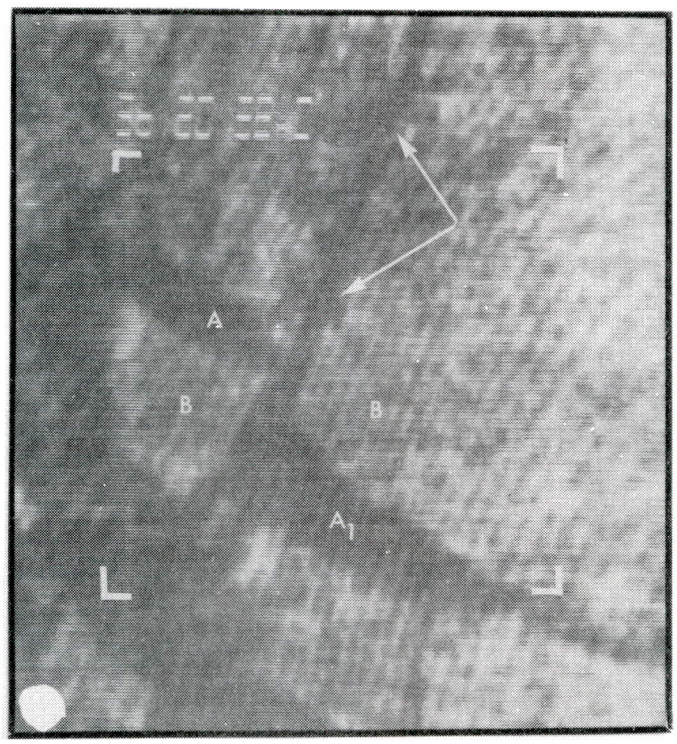

Figure 8. Thinner areas of first-year (FY) ice, (A), depicted as radiometrically warm features, are not clearly visible on the photography. There is no distinguishing feature or boundary between (A_1), and (B) on the photography.

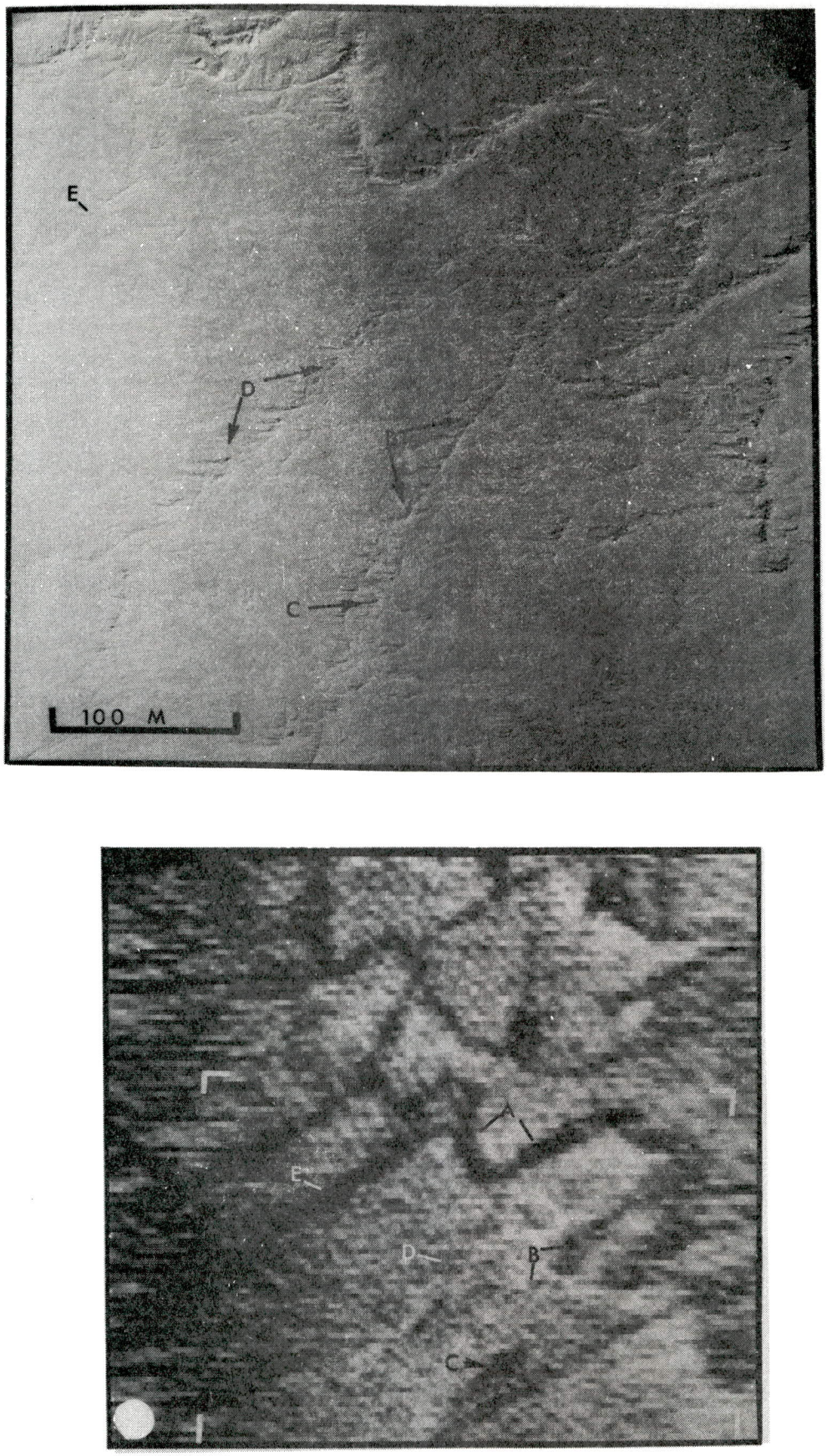

Figure 9. The ridge network can be correlated with the pattern of radiometrically warm lineations, but the higher radiation probably reflects the presence of thinner undeformed ice adjacent to the ridges. Cool radiometric lineations are indicated ridge (D).

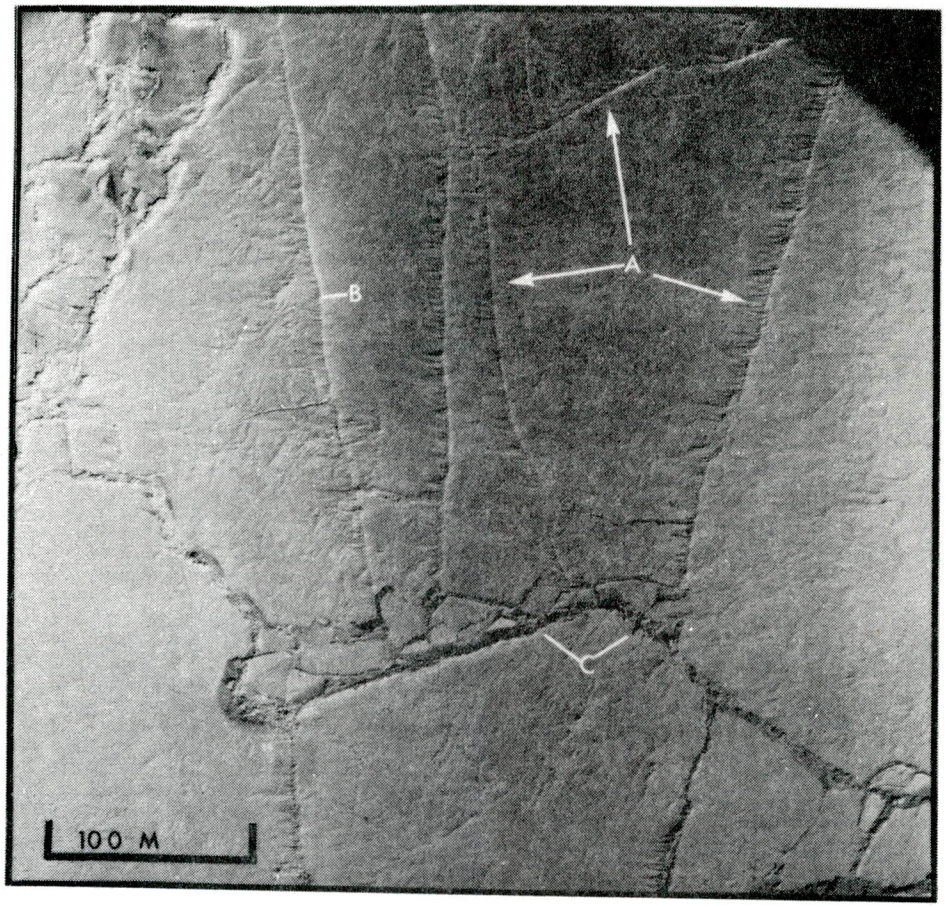

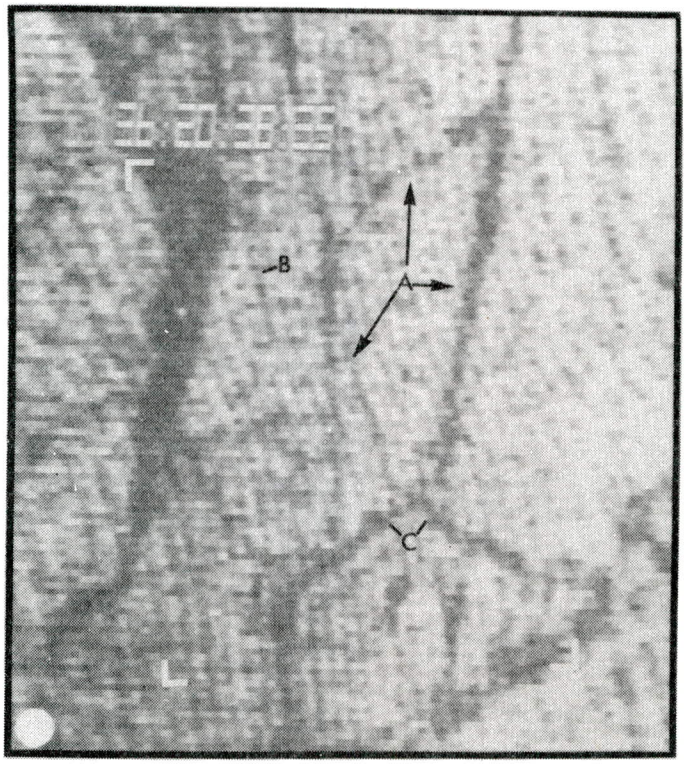

Figure 10. The warm radiometric signatures associated with the ridges (A) show a large variation in width although they appear rather uniform in width on the photographs. Ridge (B), of similar size, shows very little distinguishing signature.

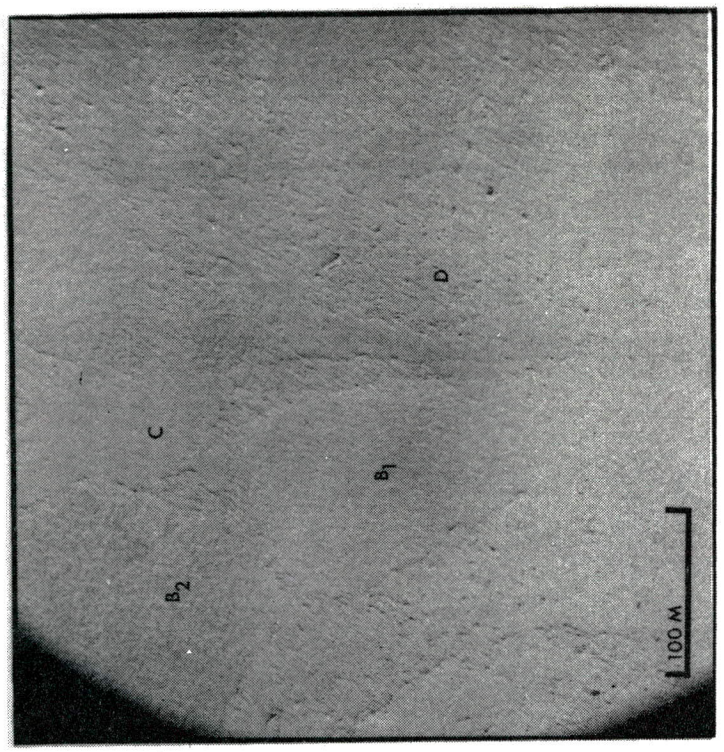

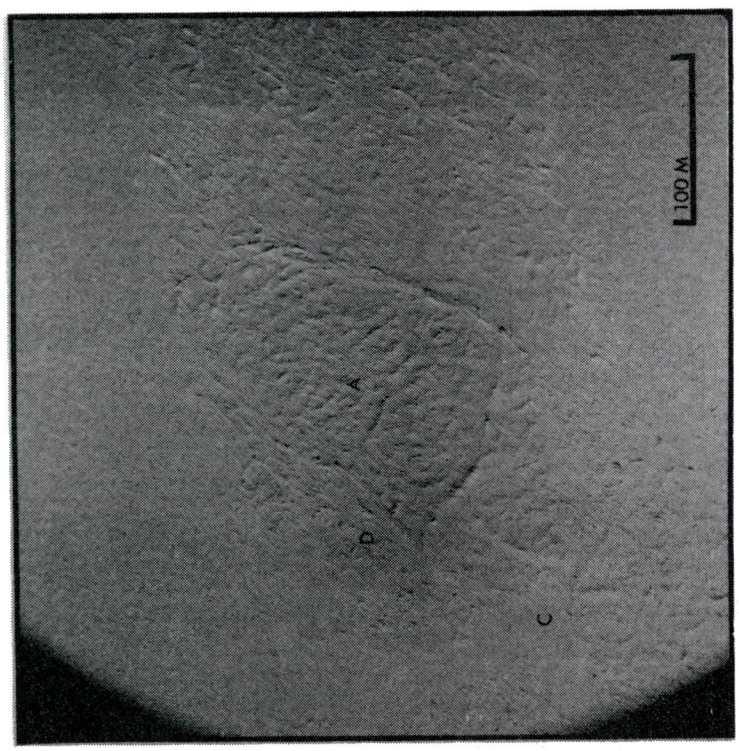

Figure 11. Arctic Basin multi-year (MY) ice floes, like (A), display brighter tones and a more splotchy texture than the Canadian Archipelago multi-year (MY) ice floes, like (B). Frozen surface melt water distribution, which produces a relatively warm T_B is more widespread on the lower relief archipelago floes.

UNCLASSIFIED

SECURITY CLASSIFICATION OF THIS PAGE *(When Data Entered)*

REPORT DOCUMENTATION PAGE		READ INSTRUCTIONS BEFORE COMPLETING FORM
1. REPORT NUMBER NORDA Technical Note 179	2. GOVT ACCESSION NO.	3. RECIPIENT'S CATALOG NUMBER
4. TITLE *(and Subtitle)* K-Band Radiometric Mapping of Sea Ice		5. TYPE OF REPORT & PERIOD COVERED Final 6. PERFORMING ORG. REPORT NUMBER
7. AUTHOR*(s)* R. D. Ketchum, Jr. L. D. Farmer J. P. Welsh, Jr.		8. CONTRACT OR GRANT NUMBER*(s)*
9. PERFORMING ORGANIZATION NAME AND ADDRESS Naval Ocean Research & Development Activity Polar Oceanography Branch NSTL Station, Mississippi 39529		10. PROGRAM ELEMENT, PROJECT, TASK AREA & WORK UNIT NUMBERS 61153N
11. CONTROLLING OFFICE NAME AND ADDRESS Naval Ocean Research & Development Activity Polar Oceanography Branch NSTL Station, Mississippi 39529		12. REPORT DATE January 1983 13. NUMBER OF PAGES 20
14. MONITORING AGENCY NAME & ADDRESS*(if different from Controlling Office)*		15. SECURITY CLASS. *(of this report)* UNCLASSIFIED 15a. DECLASSIFICATION/DOWNGRADING SCHEDULE
16. DISTRIBUTION STATEMENT *(of this Report)* Unlimited		
17. DISTRIBUTION STATEMENT *(of the abstract entered in Block 20, if different from Report)*		
18. SUPPLEMENTARY NOTES		
19. KEY WORDS *(Continue on reverse side if necessary and identify by block number)* Snow and ice Microwave Radiometer Brightness Temperature		

20. ABSTRACT *(Continue on reverse side if necessary and identify by block number)*

The Ka-band radiometric mapping system (KRMS), an airborne 33.6 GHz passive microwave imager, was flown over sea ice in the Bering, Chukchi and Beaufort Seas and in the Canadian Archipelago. The data discussed was obtained on 14 and 16 May 1982. The system, as flown, measures the relative brightness temperature (T_B) of the objects radiating toward the rotating antennae. Differences in T_B appear to be related to variation in ice thickness, surface moisture, deformation processes and melting and refreezing processes. A snow/ice

DD FORM 1 JAN 73 1473 EDITION OF 1 NOV 65 IS OBSOLETE
S/N 0102-LF-014-6601

UNCLASSIFIED

SECURITY CLASSIFICATION OF THIS PAGE *(When Data Entered)*

interface development is hypothesized to relate to decreasing T_B as ice increases in age.

The T_B of undisturbed new ice is warmer than open water. The T_B of first-year ice appears to decrease with increasing age and seems to be less variable than the thinner ice types.

Multi-year ice appears colder than first-year ice but warmer than open water. Two different categories of multi-year ice floes were observed. Arctic basin multi-year floes were distinguished by the rounded shapes, colder T_B and irregular distribution of frozen melt ponds (warmer T_B). Archipelago multi-year floes were less rounded, had warmer T_B and displayed a more regular (homogeneous) distribution of frozen melt ponds. Both categories of multi-year floes were radiometrically colder than the warmer (higher T_B) first-year ice types surrounding them and thus were readily identified.

New ice ridges were not unambiguously identified on the imagery. Ice ridges were inferred because of the observed association with warm lineations on the KRMS imagery when the ridge feature was clearly distinguished on the simultaneously obtained aerial photograph.

The imagery (hard copy) was produced in near real time, with 16 gray levels, onboard the aircraft in flight. Future processing will be digital with 256 gray levels and performed on an interactive digital image processing system.